Groundwater

Methods Note/

Integrated Surface and Subsurface Hydrological Modeling with Snowmelt and Pore Water Freeze–Thaw

by Oliver S. Schilling[1], Young-Jin Park[2], René Therrien[3], and Ranjeet M. Nagare[4]

Abstract

For the simulation of winter hydrological processes a gap in the availability of flow models existed: one either had the choice between (1) physically-based and fully-integrated, but computationally very intensive, or (2) simplified and compartamentalized, but computationally less expensive, simulators. To bridge this gap, we here present the integration of a computationally efficient representation of winter hydrological processes (snowfall, snow accumulation, snowmelt, pore water freeze–thaw) in a fully-integrated surface water-groundwater flow model. This allows the efficient simulation of catchment-scale hydrological processes in locations significantly influenced by winter processes. Snow accumulation and snowmelt are based on the degree-day method and pore water freeze–thaw is calculated with a vertical heat conduction approach. This representation of winter hydrological processes is integrated into the fully-coupled surface water-groundwater flow model HydroGeoSphere. A benchmark for pore water freeze–thaw as well as two illustrative examples are provided.

Introduction

In many areas of the world, snow accumulation, snowmelt, and pore water freezing and thawing (i.e., freeze–thaw) can significantly influence annual surface water runoff and contribute to groundwater recharge, especially during late winter and spring (Woo et al. 2000; Quinton et al. 2004; Pomeroy et al. 2007; Woo 2008; Kinar and Pomeroy 2015; Evans et al. 2018). These processes, referred to here as winter hydrological processes, are strongly controlled by air temperature. For example, winter precipitation may either be solid (snow) or liquid (rain) and fallen snow may either accumulate or melt, depending on the ambient air temperature. The snow cover can also undergo sublimation losses and redistribution by drifting (Pomeroy et al. 1998; Pomeroy et al. 2002). Spring snowmelt can generate extensive runoff, often causing floods (Waylen and Woo 1982; Cunderlik and Ouarda 2009; Zeinivand and De Smedt 2010). In areas where snowmelt is a major component of the annual hydrograph, snowmelt can be the main source of annual groundwater recharge (Hayashi et al. 2003; Berthold et al. 2004; Earman et al. 2006; Hayashi and Farrow 2014; Kinar and Pomeroy 2015; Lundberg et al. 2016). Evapotranspiration rates are low during the melting season, leading to preferential groundwater recharge from snowmelt to such an extent that the percentage that snowmelt contributes to the annual recharge may be larger than the percentage of snowfall in annual precipitation (Earman et al. 2006; Hayashi and Farrow 2014).

The awareness of the importance of winter processes for the hydrological cycle has led to efforts to simulate them both analytically and numerically (Stefan 1889;

[1]Corresponding author: Department of Geology and Geological Engineering, Université Laval, Pavillon Adrien-Pouliot, Québec, QC, G1V 0A6, Canada; oliver.schilling.1@ulaval.ca

[2]Aquanty Inc., Waterloo, Ontario, N2L 5C6, Canada

[3]Department of Geology and Geological Engineering, Université Laval, Pavillon Adrien-Pouliot, Québec, QC, G1V 0A6, Canada.

[4]ARKK Engineering Corp, 168 2301 Premier Way, Sherwood Park, AB, T8H 2K8, Canada.

Article impact statement: Computationally efficient simulations of catchment-scale winter hydrological processes in an integrated surface water-groundwater flow model.

Received August 2018, accepted October 2018.

doi: 10.1111/gwat.12841

Harlan 1973; Flerchinger and Saxton 1989; Ferguson 1999; Hansson et al. 2004; Hayashi et al. 2007; Butt and Bilal 2011; Okkonen and Kløve 2011; Endrizzi et al. 2013; Painter et al. 2016; Evans et al. 2018). The most physically accurate simulation of winter hydrological processes is currently achieved by modeling the energy and mass balance of coupled atmosphere-(land)surface-subsurface systems in an integrated manner (DeWalle and Rango 2008). However, due to the complex nonlinear processes that govern the hydrological cycle, solving the complete mass and energy balance in fully-integrated, catchment-scale hydrological models is computationally very demanding (Endrizzi et al. 2013; Painter et al. 2016). As a result, several numerical models that were designed to simulate snow accumulation and snowmelt are either based on simplified representations of parts of the hydrological cycle, or their scope is limited to either only the surface or the subsurface without the ability to integrate all hydrologically relevant components (e.g., Ferguson [1999], DeWalle and Rango [2008]). Moreover, only a few numerical models that are capable of simulating catchment-scale processes consider pore water freeze–thaw (e.g., Brookfield et al. [2009], Cherkauer and Lettenmaier [1999], Zhang et al. [2000]). Wang et al. (2009) further noted that several models rely on inadequate representations of winter processes, although they demonstrated that spring runoff simulations can be significantly improved by modeling snow accumulation, melt, and pore water freeze–thaw.

The MIKE SHE model (Graham and Butts 2005; DHI 2017) and the Hydrological Simulation Program – FORTRAN (HSPF) model (Bicknell et al. 1997) are among the models capable of simulating winter hydrologic processes in a more integrated manner. In MIKE SHE, the rate of snowmelt is calculated using the modified degree-day approach, and frozen soil is mimicked using a time-varying leakage coefficient during the early melting season. Similarly, the HSPF model provides an option to model snowmelt using the degree-day method or an energy balance approach. However, while MIKE SHE and HSPF can be linked to groundwater flow models, their flow solution is asynchronous because there is a one-way coupling between the surface and the subsurface components, without feedback between these components. Similarly, the variable density groundwater flow, heat, and mass transport model SUTRA (Voss and Provost 2010), which can simulate unsaturated flow processes and pore water freeze–thaw, requires a (one-way) coupling to a separate surface water model to allow for the inclusion of snow accumulation and melt.

Physically-based and fully-coupled surface water-groundwater (SW-GW) models, such as HydroGeoSphere (HGS) (Therrien and Sudicky 1996; Aquanty 2015) and ParFlow (Ashby and Falgout 1996), allow a synchronized two-way feedback between the surface and the subsurface. These fully-coupled hydrological models have also been coupled to land surface models (LSM) such as Noah-MP (Niu et al. 2011) or the Community Land Model (CLM) (Dai et al. 2003), which determine the frozen water content in the subsurface and the rate of snowmelt on the land surface based on an energy balance of multiple layers of soil and snow (Maxwell and Miller 2005; Kollet and Maxwell 2008; Davison et al. 2015; Davison 2016). There are thus a growing number of comprehensive and distributed hydrologic models that were formally verified and benchmarked (Maxwell et al. 2014; Kollet et al. 2017) and that are capable of simulating integrated surface and subsurface flow.

To bridge the gap between the most comprehensive two-way-coupled, but computationally intensive, and more efficient, but only one-way-coupled, hydrological models, we here present the integration of a computationally efficient representation of key winter processes (snow accumulation and snowmelt, pore water freezing and thawing) in a two-way-coupled surface water-groundwater (SW-GW) flow model. Snow accumulation and snowmelt are based on the degree-day method, which is computationally efficient. Pore water freezing and thawing are represented by an analytical solution to the one-dimensional heat conduction. This representation of winter hydrological processes was integrated in a distributed way into the two-way-coupled HGS model. The model is verified by reproducing the approximation to the Stefan equation presented by Hayashi et al. (2003), and its capabilities are demonstrated with two illustrative examples based on the widely used tilted-V catchment and Borden site (Abdul) models (Kollet et al. 2017).

Winter Hydrological Processes in HGS

The Numerical Flow Model HGS

HGS (Brunner and Simmons 2012; Aquanty 2015) is a physically-based and two-way-coupled surface water-groundwater flow model that is based on the model originally developed by Therrien and Sudicky (1996). HGS has been successfully applied in many different contexts and at many different spatial and temporal scales. Investigations on the interactions between groundwater, surface water, and vegetation (e.g., Ala-Aho et al. [2017], Schilling et al. [2014], Schomburg et al. [2018]), on the development of unsaturated zones between rivers and aquifers in heterogeneous systems (e.g., Irvine et al. [2012], Schilling et al. [2017b], Tang et al. [2017]), or on contaminant transport and tile drainage in agricultural contexts (e.g., Bonton et al. [2012], De Schepper et al. [2017]) are just some recent examples for which HGS was used. HGS has recently been coupled to the Weather Research and Forecast (WRF) model for the integrated simulation of atmosphere, surface, and subsurface interactions (Davison et al. 2015), to particle tracking and flow tracking tools (Partington et al. 2011; Partington et al. 2012; Chow et al. 2016; Schilling et al. 2017a), and to the ensemble Kalman filter (EnKF) data assimilation tool (Kurtz et al. 2017; Tang et al. 2017; Tang et al. 2018).

In HGS, surface water flow is represented with the following diffusion-wave approximation of the

two-dimensional Saint-Venant equation:

$$\frac{\partial \varphi_o h_o}{\partial t} = -\overline{\nabla} \cdot d_o \mathbf{q}_o - d_o \Gamma_{ex} \pm Q_o \quad (1)$$

where $\overline{\nabla}$ is the two-dimensional differential operator, d_o [m] is the depth of surface water (excluding rill storage height that represents microtopography), φ_o [−] is the surface flow equivalent porosity that accounts for microtopography, h_o [m] is the total head ($\equiv z + d_o$) for given water depth d_o and elevation z, $\mathbf{q}_o$ [m/d] is the average surface water flow velocity, Γ_{ex} [m/d] is the volumetric rate of fluid exchange between the surface and subsurface domains per unit surface area (positive when water flows from the surface to the subsurface), and Q_o [(m^3/d)/m^3] represents sources and sinks (volumetric flux per unit surface area). The surface flow equivalent porosity ranges between 0 and 1, depending on whether the depth of surface water is below or above the microtopography.

The average surface water flow velocity $\mathbf{q}_o$ is given by:

$$\mathbf{q}_o = -\mathbf{K}_o \cdot k_{ro} \nabla (h_o) \quad (2)$$

where k_{ro} is a dimensionless factor accounting for obstructed flow and microtopography, and $\mathbf{K}_o$ [m/d] is the surface conductance that is solved using Manning's equation.

Variably-saturated groundwater flow in HGS is simulated based on Richards' equation:

$$\frac{\partial}{\partial t} (\theta_s S_w) = -\nabla \cdot \mathbf{q} + \Gamma_{ex} \pm Q_o \quad (3)$$

where θ_s [−] is the saturated water content, S_w [−] is the water saturation, $\mathbf{q}$ [m/d] is the groundwater flux (i.e., Darcy flux), and Q_o [(m^3/d)/m^3] represents sinks and sources (volumetric flux per unit volume).

The groundwater flux $\mathbf{q}$ is given by:

$$\mathbf{q} = -k_r (S_w) \mathbf{K} \cdot \nabla (\psi_w + z) \quad (4)$$

where $k_r(S_w)$ [−] is the relative permeability of the porous medium, $\mathbf{K}$ [m/d] is the saturated hydraulic conductivity tensor of the porous medium, and ψ_w and z [m] are the pressure and the elevation head, respectively. In HGS, the relationship between the relative permeability of the porous medium, the soil water content, and pressure, can be given in tabular form or can be parametrized using the van Genuchten functions (van Genuchten 1980).

Equation 1 for surface water flow and Equation 3 for groundwater flow are fully-coupled with the dual-node approach (see de Rooij [2017]) and are solved simultaneously, without requiring iteration. HGS is based on an adaptive time stepping scheme which is optimal for the calculation of flow.

Implementation of Winter Hydrological Process in HGS

In HGS, surface and subsurface parameters can be specified separately for each individual mesh element. The same approach applies for the parameters required for the simulation of winter hydrological processes. In HGS, the depth-integrated surface water flow equation to describe the mass balance of the liquid water and snow over the land surface is given as:

$$\frac{\partial}{\partial t} \varphi_o (\rho_w d_{wv} + \rho_{snow} d_{snow}) = -\overline{\nabla} \cdot \rho_w d_o \mathbf{q}_o + \rho_w Q_o - \rho_w \Gamma_{ex} + \rho_{snow} q_{snow} \quad (5)$$

where d_{wv} [m] and ρ_w [kg/m^3] are the volume depth (actual water volume per unit area) and the density of liquid water, d_{snow} [m] and ρ_{snow} [kg/m^3] are the snow depth and the snow density, and q_{snow} [m/d] is the difference between the snowfall rate and the sublimation rate.

Efficient analytical formulations, which do not require solving the entire mass and energy balance, have been developed to circumvent the high computational demands of catchment-scale simulations of winter hydrological processes. The most widely-used analytical algorithm for the computation of snow accumulation and melt is based on the degree-day method (Rango and Martinec 1995; Ferguson 1999; DeWalle and Rango 2008), where the snowmelt rate q_{melt} [m/d] is given by:

$$q_{melt} = \alpha \cdot (T - T_c) \quad (6)$$

where α [m/(°C·d)] is the empirical degree-day factor, which can be interpreted as a melting constant, and T_c and T [°C] are the threshold and air temperature, respectively. The threshold temperature for snowmelt is typically 0 °C and the air temperature is generally assumed to be equivalent to the daily mean air temperature.

The degree-day method does not require the explicit simulation of heat transport and has been demonstrated to accurately simulate snow accumulation and melt on temporal scales of weeks to the entire winter season (Rango and Martinec 1995). Moreover, Rango and Martinec (1995) showed that coupling the degree-day method to a surface water flow model, and accounting for a variable basin-wide snow cover extent, produces results that do not differ significantly from those obtained with more complex energy balance approaches.

If the amount of snow is assumed to be determined by precipitation, and sublimation and melting by temperature change, then

$$\frac{\partial}{\partial t} \varphi_o (\rho_{snow} d_{snow}) = \rho_{snow} q_{snow} - \rho_{snow} q_{melt} (T) = \rho_{snow} \left[q_{snow} - \alpha (T - T_c) \right] \quad (7)$$

where the rate of melting is assumed to be a linear function of temperature (as in the degree-day method) with the given degree-day factor α and threshold temperature T_c [°C].

By combining the mass balance and snowmelt equations, the mass balance for the liquid phase of water is derived as

$$\frac{\partial}{\partial t}(\rho_w d_{wv}) = -\overline{\nabla}\cdot \rho_w d_f \mathbf{q}_o + \rho_w Q_o - \rho_w \Gamma_{ex} + \rho_{snow}\alpha (T - T_c) \quad (8)$$

When the temperature is known for a given snowmelt constant and threshold temperature, the snowmelt and water flow equations can be solved sequentially.

In the subsurface flow system, when the liquid phase of water can be transformed to the solid phase ice (i.e., freezing) or vice versa (i.e., thawing), the total mass of water in the system is given as $\rho_w \theta_s S_w + \rho_{ice}\theta_s S_{ice}$, where the subscripts ice represents the solid phase ice. If the ice is assumed to be immobile, then the balance of the total water mass can be described by the following equation:

$$\frac{\partial}{\partial t}(\rho_w \theta_s S_w + \rho_{ice}\theta_s S_{ice}) = \nabla\cdot \rho_w k_r (S_w)\mathbf{K}\cdot\nabla(\psi_w + z) + \rho_w Q_w \quad (9)$$

Assuming that the partitioning of water between solid and liquid phases is determined only by temperature, the following empirical relation has been suggested for the ratio of ice to the total amount of water (Andersland and Ladanyi 2004):

$$\frac{\rho_{ice} S_{ice}}{\rho_w S_w + \rho_{ice} S_{ice}} = 0 \quad \text{if} \quad T \geq T_f$$
$$\frac{\rho_{ice} S_{ice}}{\rho_w S_w + \rho_{ice} S_{ice}} = \left(\frac{T_f - T}{T_f - T_m}\right)^{\beta} \quad \text{if} \quad T_m \leq T < T_f$$
$$\frac{\rho_{ice} S_{ice}}{\rho_w S_w + \rho_{ice} S_{ice}} = 1 \quad \text{if} \quad T < T_m \quad (10)$$

where T_f and T_m are the freezing and melting temperatures. Based on experimental data, Rempel (2008) showed that the fitting parameter β[-]ranges between 0.19 and 1.15, with a mean of 0.42. If the temperature is assumed to be known at a location at a given time, the above two equations (Equations 9 and 10) can be combined to describe both the water and ice saturations.

Although Brookfield et al. (2009) successfully demonstrated the thermal energy transport in an integrated surface and subsurface system, for computational efficiency often a simple one-dimensional analytical model is employed to determine the vertical distribution of temperature in bulk porous medium (Stefan 1889; Changwei and Gough 2013). Assuming that the porous medium is homogeneous and that groundwater flow has a negligible influence on subsurface temperatures, the vertical temperature distribution can be described by the following simple conduction equation:

$$\frac{\partial}{\partial t}(T_{pm} - T_b) = \frac{\partial}{\partial z}\left(\frac{\lambda_{pm}}{c_{pm}}\frac{\partial (T_{pm} - T_b)}{\partial z}\right) \quad (11)$$

where T_{pm} [°C] is the temperature of the bulk porous medium, λ_{pm} [Wm^{-1} $°C^{-1}$] and c_{pm} [J/kg C^{-1}] are the bulk thermal conductivity and heat capacity, respectively. It is assumed that the temperature at depth is given as T_b [°C] and the surface temperature is the same as the atmospheric temperature T_{atm} [°C], such that:

$$T_{pm}(z = 0, t) = T_{atm}(t) \quad (12)$$
$$T_{pm}(z \to \infty, t) = T_b \quad (13)$$

The analytical solution of the equation is:

$$T_{pm}(z,t) = T_b + \frac{z}{\sqrt{4\pi\kappa}}\int_{\tau=0}^{t}\frac{\partial T_{atm}(\tau)}{\partial \tau} \times erfc\left[\frac{z}{\sqrt{4\tau(t-\tau)}}\right]d\tau = T_b + \frac{z}{\sqrt{4\pi\kappa}}\int_{\tau=0}^{t} T_{atm}(\tau)\frac{e^{-z^2/4\kappa(t-\tau)}}{(t-\tau)^{3/2}}d\tau \quad (14)$$

where the thermal diffusivity κ [kg/(s·m)] is defined as λ_{pm}/c_{pm}. This simple analytical solution is considered effective when the subsurface is thermally homogeneous and the influence of groundwater flow on temperature distributions is relatively weak.

Model Verification

Benchmark for Pore Water Freeze–Thaw

The most widely-used analytical algorithm for the simulation of pore water freeze–thaw is the empirical Stefan equation (Stefan 1889; Zhang et al. 2008). Stefan's equation states that latent heat released during freezing of pore water at the freezing front equals the rate at which the heat is conducted to the bulk porous medium. Stefan's equation neglects volumetric heat, which is the heat removed as ground temperatures drop to and below zero in unfrozen ground, leading to substantial reduction of frost depths in milder climates. Hayashi et al. (2007) proposed the following simple analytical form of Stefan's equation to determine the depth of the thawing front for a layered peat soil:

$$z_f = \left(\frac{2}{\rho_{ice} f L}\right)^{1/2}\cdot\left[t_0\sum(\lambda_b T_b)\right]^{1/2} \quad (15)$$

where z_f [m] is the depth to the frost table, ρ_{ice} [kg/m^3] is the density of ice, f [−] is the volumetric fraction of ice in frozen soil, L [J/kg] is the latent heat of fusion, λ_b [W/(m·°C)] is the bulk thermal conductivity of the unfrozen porous medium, and T_b [°C] is the bulk temperature of the porous medium. The time since the start of thawing is given by t_0 [s] and $\sum(\lambda_b T_b)$ is the cumulative sum of the product of the daily average λ_b and T_b.

To verify the pore water freeze–thaw process as implemented in HGS, transient simulations of the propagation of the frost table in a one-dimensional soil column

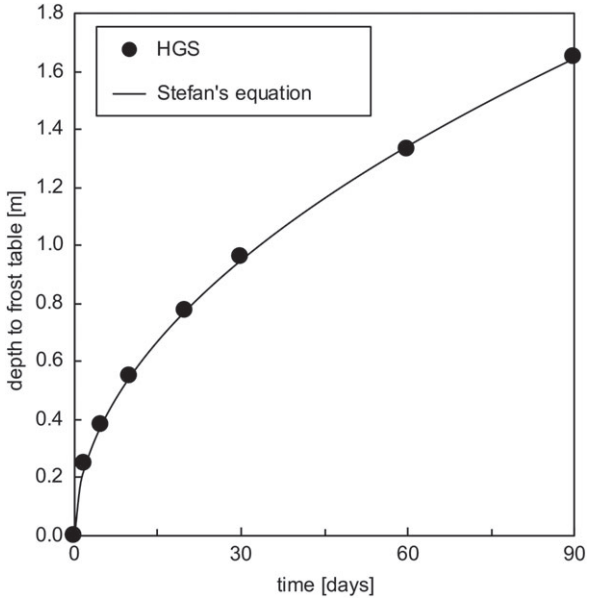

Figure 1. Development of the depth to frost table in an initially ice-saturated column calculated using Stefan's equation presented by Hayashi et al. (2007) and simulated with HGS. $R^2 = 0.995$.

initially saturated with ice are compared to calculations using Stefan's equation (Equation 15).

The HGS simulation considers a 10-m long vertical soil column that is discretized with elements whose vertical thickness is uniform and equal to 0.025 m. The soil is assumed homogeneous with a bulk thermal conductivity equal to 0.017 J/(s·cm^3·°C), a bulk heat capacity equal to 35.07 J/(cm^3·°C) and a porosity of 0.4. A uniform hydraulic head is assigned to the entire column resulting in a water-saturated column without water movement. The temperature at the bottom of the column, at a depth of 10 m, is assumed to be constant and equal to −5 °C. A constant atmospheric temperature of 10 °C is assigned to the top of the column at the start of the simulation. The total simulation time is 90 days.

The location of the frost table with time, which corresponds to the propagation of the thawing front, is illustrated in Figure 1. The figure shows excellent agreement between the HGS simulation and the calculations based on Equation 15.

Illustrative Examples

The influence of winter processes on surface water discharge is illustrated with two examples. Example 1 is based on a modified version of the tilted V-catchment model that was first proposed by Panday and Huyakorn (2004) and recently extended to allow for more substantial SW-GW interactions by Kurtz et al. (2017). Example 2 is based on a field experiment conducted by Abdul and Gillham (1989) at the Borden field site, Canada, which has been used as an inter-model comparison benchmark (Kollet et al. 2017).

Example 1: Alluvial Groundwater Pumping in a Tilted V-Catchment

The synthetic tilted V-catchment was introduced by Panday and Huyakorn (2004) to illustrate the capabilities of a coupled SW-GW flow model. It consists of a simple V-valley with a constant inclination towards the outlet. This catchment has recently been used as a benchmark for inter-model comparison (Maxwell et al. 2014; Kollet et al. 2017). The original tilted-V model was extended by Kurtz et al. (2017) to consider an aquifer of a larger vertical extent (33 m instead of only 3 m) and include two lines of four pumping wells on both sides of the stream that runs along the centerline of the tilted-V catchment. This modification allows a more realistic simulation of alluvial SW-GW interactions and the implementation of a realistic groundwater pumping scenario.

The modified tilted-V model has a spatial extent of $1620 \times 1000 \times 33$ m along the x-, y- and z-directions, respectively (Figure 2). The two valley flanks are inclined towards the center of the catchment with a slope of ± 0.05 m/m in the x-direction. The catchment is furthermore tilted in the y-direction with a slope of

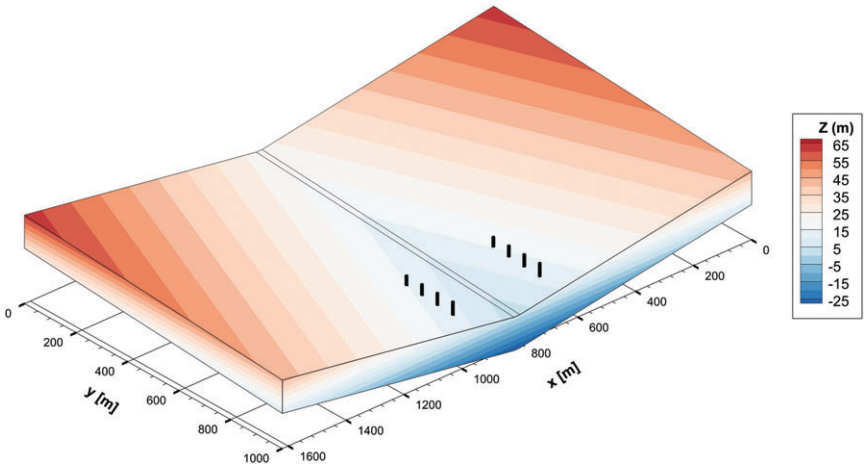

Figure 2. Modified tilted V-catchment model, after Kurtz et al. (2017). 2 x 4 groundwater wells are installed towards the outlet of the catchment (indicated by the black columns). The vertical dimension is exaggerated for better visual presentation.

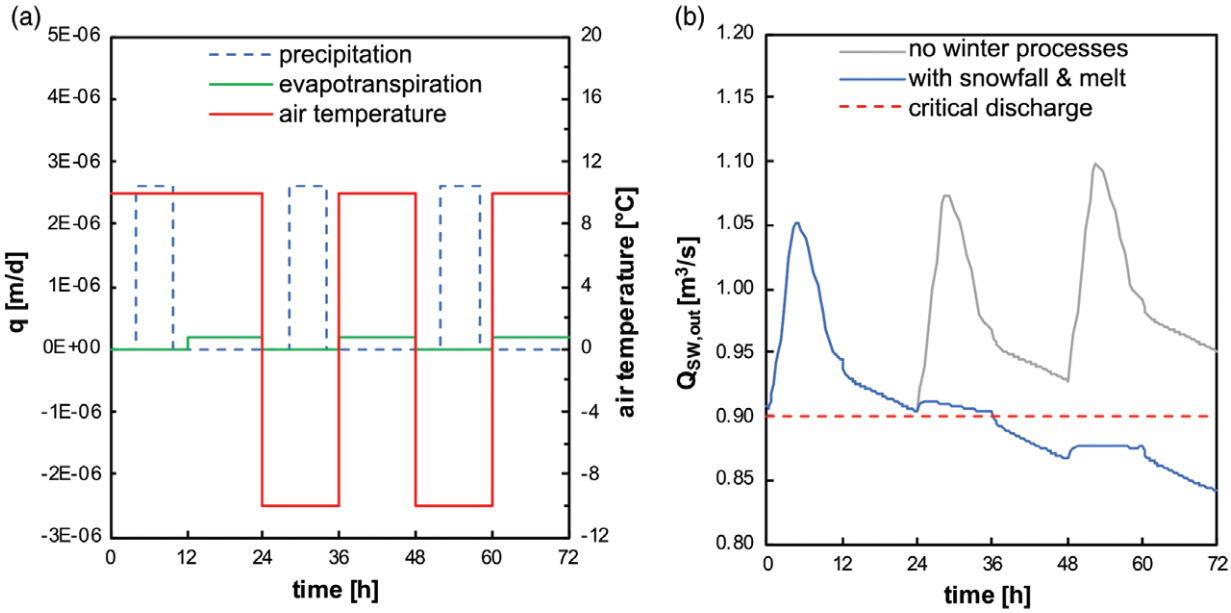

Figure 3. Modified tilted V-catchment: Time-varying input functions (a) and simulated surface water discharge at the outlet (b). In (b), a hypothetical, critical discharge of 0.9 m^3/s is indicated by the dashed red line.

0.02 m/m, forming a gently sloping stream along the centerline of the valley. The catchment is discretized in HGS with 3D rectangular prism elements, with a uniform element size equal to 20 m in the x- and y-directions. A total of 10 layers of elements are used to discretize the catchment in the vertical z-direction, with the following decreasing element thicknesses, from bottom to top: 10, 10, 6, 3, 2, 1.1, 0.5, 0.25, 0.1, and 0.5 m. The resulting mesh has a total of $80 \times 50 \times 11$ nodes along the x-, y- and z-directions, respectively.

The modified tilted-V catchment with alluvial drinking water production is a typical setup in mountainous and peri-alpine catchments, where winter processes play a key role (Kurtz et al. 2017; Schilling et al. 2017a). If winter processes are not taken into account when managing groundwater pumping stations in such systems, during the winter season groundwater abstraction may exceed sustainable amounts because recharge is strongly reduced by the retention of precipitation as snow. To demonstrate the importance of simulating snowfall, snow accumulation, and melt for the management of a groundwater pumping station, two different scenarios were considered. In scenario 1, all precipitation was simulated as rain and winter hydrological processes were not considered, which made precipitation immediately available for surface water runoff and groundwater recharge. In scenario 2, winter hydrological processes were considered: precipitation was simulated as rain or snow depending on the atmospheric temperature, and snow accumulation and melt were considered. Freezing and thawing of the subsurface were not considered. Precipitation could thus be temporally stored as snow and was not always immediately available for surface water runoff and groundwater recharge.

The simulation period was set to 3 days. For both scenarios, three precipitation events of 0.0026 mm water equivalent/day and a duration of 6 h each (04:00–10:00 each day) were simulated. A diurnally varying evapotranspiration rate of 0 from 00:00 to 12:00 and 0.0002 mm/day from 12:00 to 24:00 was applied for both scenarios. In the winter hydrological processes scenario (scenario 2), the model was additionally forced with diurnal temperature variations of $-10\,^{\circ}$C from 00:00 to 12:00 and $10\,^{\circ}$C from 12:00 to 24:00, starting on the second day of simulation. The temperature forcing was set constant over a minimum of 12 h in order to accommodate for the fact that the degree day method works best when daily average temperatures are used. To facilitate the presentation of the effects of snow accumulation and melt on the behavior of the catchment outflow, sublimation was set to 0 for the entire simulation period. The time-varying input functions are illustrated in Figure 3a.

The modified tilted-V model was simulated under consideration of variably-saturated groundwater flow. A constant hydraulic head equal to 23.2 m was assigned to the upstream boundary of the model, at $y = 0$ m, providing a temporally uniform regional groundwater inflow as well as a base flow within the channel. A critical depth boundary condition was applied to the surface nodes at the catchment outlet, located at $y = 1000$ m. The lateral boundaries, at $x = 0$ m and $x = 1620$ m, and the bottom boundary were assumed to be impermeable. Groundwater was abstracted at a constant rate of 0.46 m^3/day through each of the eight groundwater pumps. Hydraulic properties are listed in Table 1 and were applied uniformly in the model.

The resulting surface water discharge at the outlet ($Q_{SW,out}$) is illustrated in Figure 3b**,** along with a critical discharge value of 0.9 m^3/s that could, for example,

Table 1
Model Parameters for the Tilted-V Catchment Model

Variable	Value	Unit
Saturated hydraulic conductivity	2.9×10^{-3}	m/s
Porosity	0.43	$m^3\ m^{-3}$
van Genuchten α	3.48	m^{-1}
van Genuchten β	1.75	—
Residual saturation	0.05	$m^3\ m^{-3}$
Manning's coefficient	0.15	$s/m^{1/3}$
Coupling length	1×10^{-7}	m
Rill storage height	0.1	m
Snow density	100	kg/m^3
Melting constant	5	mm(snow) $d^{-1}\ °C^{-1}$
Sublimation constant	0	mm(snow) d^{-1}
Threshold temperature	0	°C
Initial snow depth	0	m

Table 2
Model Parameters of the Borden Site Model

Variable	Value	Unit
Saturated hydraulic conductivity	1×10^{-5}	m/s
Porosity	0.34	$m^3\ m^{-3}$
van Genuchten α	1.9	m^{-1}
van Genuchten β	6	—
Residual saturation	0.18	$m^3\ m^{-3}$
Manning's coefficient (plot/channel)	0.3/0.03	$s/m^{1/3}$
Coupling length	0.1	m
Rill storage height	0.002	m
Initial water table elevation	2.78	m
Snow density	100	kg/m^3
Melting constant	5	mm(snow) $d^{-1}\ °C^{-1}$
Sublimation constant	0	mm(snow) d^{-1}
Threshold temperature	0	°C
Initial snow depth	0.1	m
Thermal diffusivity	2×10^{-7}	m^2/d
Background temperature	6	°C
Melting temperature	−0.5	°C
Freezing temperature	0.5	°C
Maximum freezing depth	2	m

represent a hypothetical minimum discharge that needs to be maintained. For scenario 1 without winter hydrological processes, the surface water discharge never falls below this critical minimum discharge. For scenario 2, where at the onset of the second day precipitation falls in the form of snow that accumulates on the hillslopes, the surface water discharge rapidly drops below the critical value of 0.9 m^3/s and, subsequently, does not recover.

This illustrative example highlights that (1) winter hydrological processes can play an important role in the context of drinking water supply, and that (2) the simulation of snowfall, snow accumulation and melt in HGS may substantially improve the management of groundwater pumping

Example 2: Seasonal Hydrograph Response

For the second illustrative example, a seasonal hydrograph response is simulated using a model based on a field experiment conducted at the Borden research site (Abdul and Gillham 1989; Kollet et al. 2017). The Borden field site model, illustrated in Figure 4, represents a small, shallow aquifer with a depth of about 4 m and a horizontal extent of about 20 m by 80 m.

The simulation domain is discretized with 1372 nodes and 2651 triangular elements. The 3D model consists of 15 layers, resulting in 39,765 triangular prism elements. The hydraulic parameters of the Borden site model are listed in Table 2.

Variably-saturated groundwater flow was considered for the Borden site model. The lateral and bottom subsurface boundaries were set impermeable. Surface water outflow was simulated through a critical depth

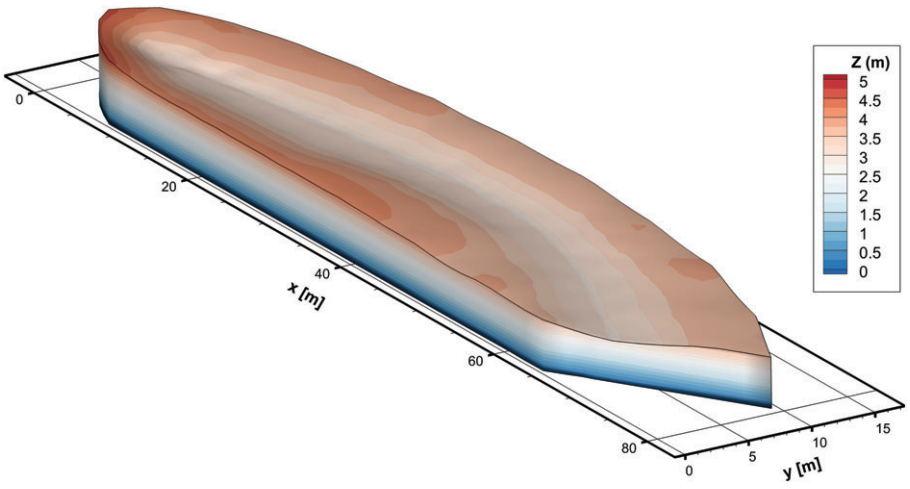

Figure 4. The Borden site model, modified after Abdul and Gillham (1989).

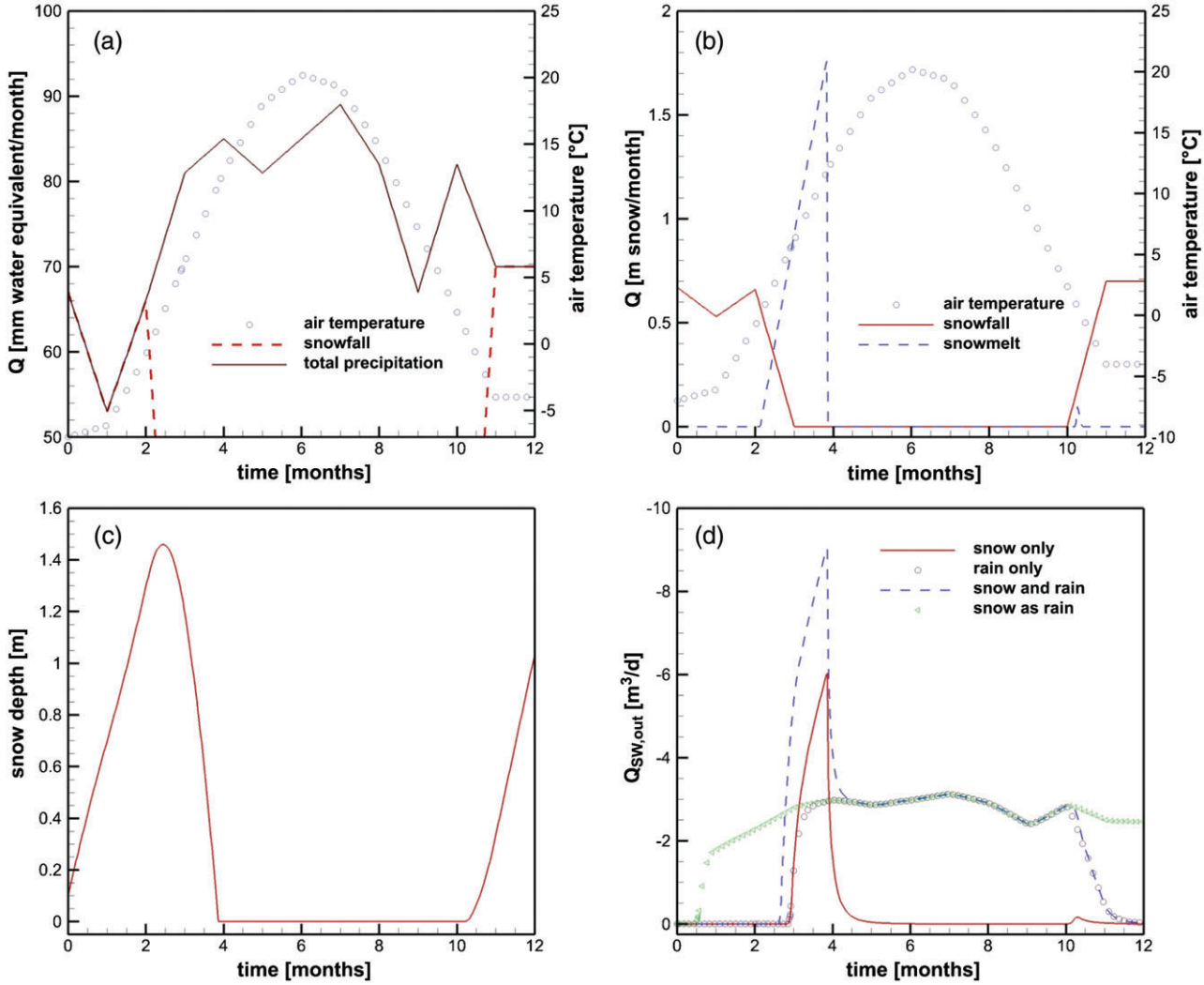

Figure 5. Borden site model inputs and outputs. (a) Comparison of air temperature, snowfall, and total precipitation model inputs of scenario "snow and rain." (b) Simulated air temperature, snowfall, and snowmelt of scenario "snow and rain." (c) Simulated snow depth of scenario "snow and rain." (d) Simulated stream discharge at the outlet of the catchment ($Q_{SW,out}$) of the four model scenarios: simulation only of the snow component of the annual precipitation ("snow only"), simulation only of the rain component of the precipitation ("rain only"), simulation of the entire annual precipitation under consideration winter hydrological processes ("snow and rain"), and simulation of the entire annual precipitation without the consideration of winter hydrological processes ("snow as rain").

boundary condition at surface nodes located at the downstream model boundary (towards the corner of $x = 80$, $y = 0$). Whereas in the groundwater abstraction example only snowfall, snow accumulation, and snowmelt were considered, in this example pore water freeze–thaw was included as well. Example 2 was set up such that the influence of winter hydrological processes on the different streamflow components can be illustrated. For this purpose, four different simulation scenarios were compared: In scenario 1, all precipitation was simulated as rain and winter hydrological processes were not considered (scenario "snow as rain"). In scenario 2, all winter processes were considered (snowfall, snow accumulation, snowmelt) and pore water freeze–thaw was also simulated (scenario "snow and rain"). Sublimation was turned off for improved visual presentation. In scenario 3, winter processes were not considered, and the model was forced only by the summer rain component (scenario "rain only"). In scenario 4, winter processes were considered but only the winter snow component was used to force the model (scenario "snow only"). The time-varying precipitation and air temperature boundary conditions are illustrated in Figure 5a.

The results of the different simulations are illustrated in Figure 5c and 5d and Figure 6: In Figure 5b, snowfall and air temperature are compared to the amount of snowmelt simulated for the scenario with all winter hydrological processes ("snow and rain"). In Figure 5c the simulated snow depth of the "snow and rain" scenario throughout the course of a year is shown. In Figure 5d, the surface water discharge for the different simulation scenarios is illustrated. As can be seen from the discharge hydrographs (Figure 5d), neglecting winter processes and simulating snow as rain would result in an almost

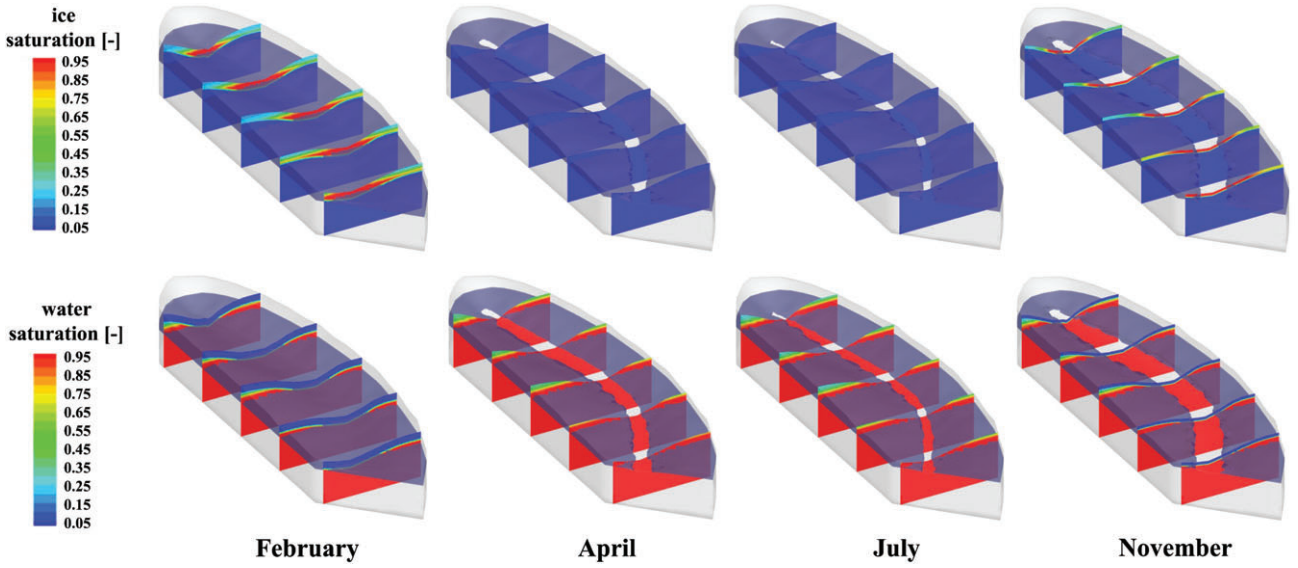

Figure 6. Cross-sectional view of simulated ice (top row) and water saturation (bottom row) at four discrete points in time (February, April, July, and November). The model domain is indicated by the shaded gray box.

uniform discharge response at the outlet of the catchment. However, under consideration of winter processes, the discharge hydrograph reflects typical responses in catchments influenced by winter processes: There is very low to zero discharge during winter months as a result of snow accumulation during winter which can be seen in Figure 5c. During spring when the accumulated snow melts (see Figure 5c), surface water discharge peaks (see Figure 5d). After spring, surface water discharge is significantly reduced to a relatively uniform amount throughout the summer months. Discharge reaches low flow conditions at the onset of winter once precipitation starts to be stored on the surface as snow.

The simulated ice saturation in the subsurface of four selected months of the year is provided in Figure 6, along with water saturation in the subsurface. The top row of Figure 6 illustrates the effect of freeze–thaw on groundwater flow: Groundwater flow is blocked underneath the channel in the center of the Borden site due to very pronounced subsurface freeze in February. Groundwater flow is only possible at shallow depths during spring and summer, when no parts of the soil are frozen (e.g., April and July). However, the shallow soils become frozen again at the onset of winter in November, which again effectively blocks groundwater flow at shallow depths. Soil saturation, illustrated in the bottom row of Figure 6, is also strongly affected by winter processes: In February, the topsoil is nearly completely desaturated because precipitation is retained on the surface as snow and recharge is limited. During spring and summer months (April and July), the topsoil is partially saturated as a result of recharge processes. With the onset of winter (November), topsoil saturation starts to decrease again due to the retention of precipitation as snow on the surface and the beginning of freezing in the topsoil.

Discussion and Conclusions

Many regions on Earth are strongly influenced by winter processes, and the interplay between snow accumulation, snowmelt and pore water freeze–thaw is a major driver for hydrological systems in these regions. As demonstrated in the idealized but illustrative examples, neglecting winter hydrological processes in surface water and groundwater flow simulations results in substantially different hydrographs, overestimating surface water discharge and groundwater recharge in winter months and underestimating the potential for flooding during the snowmelt period. However, the simple and computationally effective implementation of winter hydrological processes in HGS allows typical hydrograph responses of winter-influenced catchments to be reproduced, both on the daily as well as on the seasonal scale.

As Evans and Ge (2017) and Evans et al. (2018) demonstrated with their groundwater flow simulations that took heat transport and soil freeze–thaw into account, not only surface water discharge but also groundwater discharge is influenced by winter hydrological processes: groundwater discharge is likely going to increase in the future as a result of a warming climate, because increased temperatures are able to decrease the amount and duration of frozen soils, which in turn may alter the timing and amount of recharge and of groundwater discharge. Rather than relying on preprocessing of precipitation data into recharge from snowmelt, as was required for the simulations by Evans et al. (2018), the integration of snow accumulation, snowmelt, and freeze–thaw in HGS is able to efficiently reproduce this behavior of soil freeze and recharge in a physically-based and fully-coupled way without the need for preprocessing.

The water management tools used for predicting the behavior of surface water and groundwater in winter influenced regions need to reflect the relevant winter

hydrological processes. Where groundwater is pumped from alluvial aquifers that are fed by rivers under strong winter hydrological influence, as is the case for countries in alpine regions, the interplay between groundwater, river water, rain, and snow has to be simulated under consideration of winter hydrological process for optimal water resources management. Predicting the behavior of coupled and dynamic SW-GW systems that are used for drinking water production with physically-based models that consider all relevant processes becomes even more important under the influence of climate change, of which the impacts to our drinking water supplies are already starting to become apparent.

The integration of winter hydrological processes in the fully-coupled flow model HGS allows the consideration of all relevant processes in a physically-based and computationally efficient way. This integrated approach for the simulation of winter hydrological processes significantly simplifies obtaining reliable predictions of surface water and groundwater fluxes, as it allows the use of measured data without requiring any transformation or preprocessing such as separating measured precipitation into liquid and solid precipitation, or transforming measured precipitation into snow, snowmelt, and recharge from snowmelt. Most relevant data required for winter hydrological simulations with HGS are readily available, and there is no extra effort involved in setting up an integrated SW-GW model for winter-influenced catchments. With the efficient implementation of winter hydrological processes into HGS, intra- as well as inter-annual simulations of small catchments under the influence of winter can be undertaken on normal desktop machines, and more complex simulations, for example of large catchments under climate change scenarios, can be simulated on computational cloud infrastructure (Kurtz et al. 2017; Cochand et al. 2018). The representation of winter hydrological processes in HGS relies on some simplifying assumptions, such as uniform thermal properties and negligible heat transfer by convection in the subsurface. Future work is planned to modify the model to fully couple the fluid flow and energy transfer equations and evaluate the impact of these simplifying assumptions.

Acknowledgments

O.S.S. gratefully acknowledges the funding provided by the Swiss National Science Foundation (SNSF, grant no. P2NEP2_171985). R.T. also acknowledges support from the Natural Sciences and Engineering Research Council of Canada. We thank the executive editor Yu-Feng Lin, as well as Michael Fienen and two anonymous reviewers for insightful comments that have contributed to improve the paper.

References

Abdul, A.S., and R.W. Gillham. 1989. Field studies of the effects of the capillary-fringe on streamflow generation. *Journal of Hydrology* 112, no. 1–2: 1–18. https://doi.org/10.1016/0022-1694(89)90177-7

Ala-Aho, P., C. Soulsby, H. Wang, and D. Tetzlaff. 2017. Integrated surface-subsurface model to investigate the role of groundwater in headwater catchment runoff generation: A minimalist approach to parameterisation. *Journal of Hydrology* 547: 664–677. https://doi.org/10.1016/j.jhydrol.2017.02.023

Andersland, O.B., and B. Ladanyi. 2004. *Frozen Ground Engineering*, 2nd ed. Reston, VA: American Society of Civil Engineers, John Wiley & Sons.

Aquanty. 2015. *HydroGeoSphere: A Three-Dimensional Numerical Model Describing Fully-Integrated Subsurface and Surface Flow and Solute Transport*. Waterloo, ON, Canada: Aquanty.

Ashby, S.F., and R.D. Falgout. 1996. A parallel multigrid preconditioned conjugate grandient algorithm for groundwater flow simulations. *Nuclear Science and Engineering* 124: 145–159.

Berthold, S., L.R. Bentley, and M. Hayashi. 2004. Integrated hydrogeological and geophysical study of depression-focused groundwater recharge in the Canadian prairies. *Water Resources Research* 40, no. 6. https://doi.org/10.1029/2003WR002982

Bicknell, B. R., Imhoff, J. C., Kittle, J. L. J., Donigian, A. S. J., & Johanson, R. C. (1997). *Hydrological Simulation Program--Fortran, User's manual for version 11*. Retrieved from Athens, GA, USA:

Bonton, A., C. Bouchard, A. Rouleau, M.J. Rodriguez, and R. Therrien. 2012. Calibration and validation of an integrated nitrate transport model within a well capture zone. *Journal of Contaminant Hydrology* 18: 1–18. https://doi.org/10.1016/j.jconhyd.2011.10.007

Brookfield, A.E., E.A. Sudicky, Y.-J. Park, and B. Conant. 2009. Thermal transport modelling in a fully integrated surface/subsurface framework. *Hydrological Processes* 23, no. 15: 2150–2164. https://doi.org/10.1002/hyp.7282

Brunner, P., and C.T. Simmons. 2012. HydroGeoSphere: A fully integrated, physically based hydrological model. *Ground Water* 50, no. 2: 170–176. https://doi.org/10.1111/j.1745-6584.2011.00882.x

Butt, M.J., and M. Bilal. 2011. Application of snowmelt runoff model for water resource management. *Hydrological Processes* 25, no. 24: 3735–3747. https://doi.org/10.1002/hyp.8099

Changwei, X., and W.A. Gough. 2013. A simple ThawFreeze algorithm for a multi-layered soil using the Stefan equation. *Permafrost Periglacial Process* 24, no. 3: 252–260. https://doi.org/10.1002/ppp.1770

Cherkauer, K.A., and D. Lettenmaier. 1999. Hydrologic effects of frozen soils in the upper Mississippi River basin. *Journal of Geophysical Research – Atmospheres* 104, no. D16: 19599–19610. https://doi.org/10.1029/1999JD900337

Chow, R., M.E. Frind, E.O. Frind, J.P. Jones, M.R. Sousa, D.L. Rudolph, J.W. Molson, and W. Nowak. 2016. Delineating baseflow contribution areas for streams – A model and methods comparison. *Journal of Contaminant Hydrology* 195: 11–22. https://doi.org/10.1016/j.jconhyd.2016.11.001

Cochand, F., R. Therrien, and J.-M. Lemieux. 2018. Integrated hydrological modeling of climate change impacts in a snow-influenced catchment. *Groundwater*.

Cunderlik, J.M., and T.B. Ouarda. 2009. Trends in the timing and magnitude of floods in Canada. *Journal of Hydrology* 375, no. 3: 471–480. https://doi.org/10.1016/j.jhydrol.2009.06.050

Dai, Y., X. Zeng, R. Dickinson, I. Baker, G.B. Bonan, M.G. Bosilovich, A.S. Denning, P.A. Dirmeyer, P.R. Houser, G.Y. Niu, K.W. Oleson, C.A. Schlosser, and Z.-L. Yang. 2003. The common land model. *Bulletin of the American Meteorological Society* 84, no. 8: 1013–1023. https://doi.org/10.1175/BAMS-84-8-1013

Davison, J. H. (2016). *Incorporating Advanced Surface and Subsurface Processes in Mesoscale Climate Models*. (PhD), University of Waterloo, Waterloo, Canada.

Davison, J.H., H.T. Hwang, E.A. Sudicky, and J.C. Lin. 2015. Coupled atmospheric, land surface, and subsurface modeling: Exploring water and energy feedbacks in three dimensions. *Advances in Water Resources* 86: 73–85. https://doi.org/10.1016/j.advwatres.2015.09.002

De Schepper, C., R. Therrien, J.C. Refsgaard, X. He, C. Kjaergaard, and B.V. Iversen. 2017. Simulating seasonal variations of tile drainage discharge in an agricultural catchment. *Water Resources Research* 53: 3896–3920. https://doi.org/10.1002/2016WR020209

DeWalle, D.R., and A. Rango. 2008. *Principles of Snow Hydrology*. Cambridge, UK: Cambridge University Press.

DHI. 2017. *MIKE SHE*. Hørsholm, Denmark: DHI.

Earman, S., A.R. Campbell, F.M. Phillips, and B.D. Newman. 2006. Isotopic exchange between snow and atmospheric water vapor: Estimation of the snowmelt component of groundwater recharge in the southwestern United States. *Journal of Geophysical Research–Atmospheres* 111, no. D9: 1–18. https://doi.org/10.1029/2005JD006470

Endrizzi, S., S. Gruber, M. Dall'Amico, and R. Rigon. 2013. GEOtop 2.0.: Simulating the combined energy and water balance at and below the land surface accounting for soil freezing, snow cover and terrain effects. *Geoscientific Model Development* 7, no. 6: 2831–2857. https://doi.org/10.5194/gmdd-6-6279-2013

Evans, S.G., and S. Ge. 2017. Contrasting hydrogeologic responses to warming in permafrost and seasonally frozen ground hillslopes. *Geophysical Research Letters* 44: 1803–1813. https://doi.org/10.1002/2016GL072009

Evans, S.G., S. Ge, C.I. Voss, and N.P. Molotch. 2018. The role of frozen soil in groundwater discharge predictions for warming alpine watersheds. *Water Resources Research* 54: 1599–1615. https://doi.org/10.1002/2017WR022098

Ferguson, R.I. 1999. Snowmelt runoff models. *Progress in Physical Geography* 23, no. 2: 205–227.

Flerchinger, G.N., and K.E. Saxton. 1989. Simultaneous heat and water model of a freezing snow-residue-soil system: I. Theory and development. *Transactions of the American Society of Agricultural Engineers* 32, no. 2: 565–571.

van Genuchten, M.T. 1980. A closed-form equation for predicting the hydraulic conductivity of unsaturated soils. *Soil Science Society of America Journal* 44: 892–898.

Graham, D.N., and M.B. Butts. 2005. Flexible, integrated watershed modelling with MIKE SHE. In *Watershed Models*, ed. V.P. Singh, and D.K. Frevert, 245–272. Boca Raton, FL: Taylor and Francis.

Hansson, K., J. Simunek, M. Mizoguchi, L.-C. Lundin, and M.T. van Genuchten. 2004. Water flow and heat transport in frozen soil. *Vadose Zone Journal* 3, no. 2: 693–704. https://doi.org/10.2136/vzj2004.0693

Harlan, R.L. 1973. Analysis of coupled heat-fluid Transporitn partially frozen soil. *Water Resources Research* 9, no. 5: 1314–1323.

Hayashi, M., and C.R. Farrow. 2014. Watershed-scale response of groundwater recharge to inter-annual and inter-decadal variability in precipitation (Alberta, Canada). *Hydrogeology Journal* 22, no. 8: 1825–1839. https://doi.org/10.1007/s10040-014-1176-3

Hayashi, M., G. van der Kamp, and R. Schmidt. 2003. Focused infiltration of snowmelt water in partially frozen soil under small depressions. *Journal of Hydrology* 270, no. 3: 214–229. https://doi.org/10.1016/S0022-1694(02)00287-1

Hayashi, M., N. Goeller, W.L. Quinton, and N. Wright. 2007. A simple heat-conduction method for simulating the frost-table depth in hydrological models. *Hydrological Processes* 21, no. 19: 2610–2622. https://doi.org/10.1002/hyp.6792

Irvine, D.J., P. Brunner, H.-J. Hendricks Franssen, and C.T. Simmons. 2012. Heterogeneous or homogeneous? Implications of simplifying heterogeneous streambeds in models of losing streams. *Journal of Hydrology* 424-425: 16–23. https://doi.org/10.1016/j.jhydrol.2011.11.051

Kinar, N.J., and J.W. Pomeroy. 2015. Measurement of the physical properties of the snowpack. *Reviews of Geophysics* 53: 481–544. https://doi.org/10.1002/2015RG000481

Kollet, S.J., and R.M. Maxwell. 2008. Capturing the influence of groundwater dynamics on land surface processes using an integrated, distributed watershed model. *Water Resources Research* 44, no. 2. https://doi.org/10.1029/2007WR006004

Kollet, S.J., M. Sulis, R.M. Maxwell, C. Paniconi, M. Putti, G. Bertoldi, E.T. Coon, E. Cordano, S. Endrizzi, E. Kikinzon, E. Mouche, C. Mügler, Y.-J. Park, J.C. Refsgaard, S. Stisen, and E.A. Sudicky. 2017. The integrated hydrologic model intercomparison project, IH-MIP2: A second set of benchmark results to diagnose integrated hydrology and feedbacks. *Water Resources Research* 53: 867–890. https://doi.org/10.1002/2016WR019191

Kurtz, W., A. Lapin, O.S. Schilling, Q. Tang, E. Schiller, T. Braun, D. Hunkeler, H. Vereecken, E.A. Sudicky, P. Kropf, H.-J. Hendricks Franssen, and P. Brunner. 2017. Integrating hydrological modelling, data assimilation and cloud computing for real-time management of water resources. *Environmental Modelling and Software* 93: 418–135. https://doi.org/10.1016/j.envsoft.2017.03.011

Lundberg, A., P. Ala-Aho, O.M. Eklo, B. Klöve, J. Kværner, and C. Stumpp. 2016. Snow and frost: Implications for spatiotemporal infiltration patterns – A review. *Hydrological Processes* 30: 1230–1250. https://doi.org/10.1002/hyp.10703

Maxwell, R.M., and N.L. Miller. 2005. Development of a coupled land surface groundwater model. *Journal of Hydrometeorology* 6, no. 3: 233–247. https://doi.org/10.1175/JHM422.1

Maxwell, R.M., M. Putti, S. Meyerhoff, J.-O. Delfs, I.M. Fergusson, V. Ivanov, J. Kim, O. Kolditz, S.J. Kollet, M. Kumar, S. Lopez, J. Niu, C. Paniconi, Y.-J. Park, M.S. Phanikumar, C. Shen, E.A. Sudicky, and M. Sulis. 2014. Surface-subsurface model intercomparison: A first set of benchmark results to diagnose integrated hydrology and feedbacks. *Water Resources Research* 50: 1531–1549. https://doi.org/10.1002/2013WR013725

Niu, G.Y., Z.L. Yang, K.E. Mitchell, F. Chen, M.B. Ek, M. Barlage, A. Kumar, K. Manning, D. Niyogi, E. Rosero, and M. Tewari. 2011. The community Noah land surface model with multiparameterization options (Noah-MP): 1. Model description and evaluation with local-scale measurements. *Journal of Geophysical Research – Atmospheres* 116, no. D12: 116. https://doi.org/10.1029/2010JD015139

Okkonen, J., and B. Kløve. 2011. A sequential modelling approach to assess groundwater–surface water resources in a snow dominated region of Finland. *Journal of Hydrology* 411: 91–107. https://doi.org/10.1016/j.jhydrol.2011.09.038

Painter, S.L., E.T. Coon, A.L. Atchley, M. Berndt, R. Garimella, J.D. Moulton, D. Svyatskiy, and C.J. Wilson. 2016. Integrated surface/subsurface permafrost thermal hydrology: Model formulation and proof-of-concept simulations. *Water Resources Research* 52: 6062–6077. https://doi.org/10.1002/2015WR018427

Panday, S., and P.S. Huyakorn. 2004. A fully coupled physically-based spatially-distributed model for evaluating surface/subsurface flow. *Advances in Water Resources* 27: 361–382. https://doi.org/10.1016/j.advwatres.2004.02.016

Partington, D., P. Brunner, C.T. Simmons, R. Therrien, A.D. Werner, G.C. Dandy, and H.R. Maier. 2011. A hydraulic mixing-cell method to quantify the groundwater component of streamflow within spatially distributed fully integrated surface water groundwater flow models. *Environmental Modelling and Software* 26: 886–898. https://doi.org/10.1016/j.envsoft.2011.02.007

Partington, D., P. Brunner, C.T. Simmons, A.D. Werner, R. Therrien, H.R. Maier, and G.C. Dandy. 2012. Evaluation of outputs from automated baseflow separation methods against simulated baseflow from a physically based, surface water-groundwater flow model. *Journal of Hydrology* 458-459: 28–39. https://doi.org/10.1016/j.jhydrol.2012.06.029

Pomeroy, J.W., D.M. Gray, K.R. Shook, B. Toth, R.L.H. Essery, A. Pietroniro, and N.R. Hedstrom. 1998. An evaluation of snow accumulation and ablation processes for land surface modelling. *Hydrological Processes* 12: 2339–2367.

Pomeroy, J.W., D.M. Gray, N.R. Hedstrom, and J.R. Jancowicz. 2002. Prediction of seasonal snow accumulation in cold climate forests. *Hydrological Processes* 16: 3543–3558. https://doi.org/10.1002/hyp.1228

Pomeroy, J.W., D.M. Gray, T. Brown, N.R. Hedstrom, W.L. Quinton, R.J. Granger, and S.K. Carey. 2007. The cold regions hydrological model: A platform for basing process representation and model structure on physical evidence. *Hydrological Processes* 21, no. 19: 2650–2667. https://doi.org/10.1002/hyp.6787

Quinton, W.L., S.K. Carey, and N.T. Goeller. 2004. Snowmelt runoff from northern alpine tundra hillslopes: Major processes and methods of simulation. *Hydrology and Earth System Sciences* 8, no. 5: 877–890. https://doi.org/10.5194/hess-8-877-2004

Rango, A., and J. Martinec. 1995. Revisiting the degree-day method for snowmelt computations. *Journal of the American Water Resources Association* 31, no. 4: 657–669. https://doi.org/10.1111/j.1752-1688.1995.tb03392.x

Rempel, A.W. 2008. A theory for ice till interactions and sediment entrainment beneath glaciers. *Journal of Geophysical Research* 113, no. F1: 1–20. https://doi.org/10.1029/2007JF000870

de Rooij, R. 2017. A consistent implementation of the dual node approach for coupling surface-subsurface flow and its comparison to the common node approach. *Hydrology and Earth System Sciences Discussions* 21: 5709–5724. https://doi.org/10.5194/hess-2017-168

Schilling, O.S., J. Doherty, W. Kinzelbach, H. Wang, P.N. Yang, and P. Brunner. 2014. Using tree ring data as a proxy for transpiration to reduce predictive uncertainty of a model simulating groundwater–surface water– vegetation interactions. *Journal of Hydrology* 519: 2258–2271. https://doi.org/10.1016/j.jhydrol.2014.08.063s

Schilling, O.S., C. Gerber, D.J. Partington, R. Purtschert, M.S. Brennwald, R. Kipfer, D. Hunkeler, and P. Brunner. 2017a. Advancing physically-based flow simulations of alluvial systems through observations of 222Rn, 3H/3He, atmospheric noble gases and the novel 37Ar tracer method. *Water Resources Research* 53, no. 12: 10465–10490. https://doi.org/10.1002/2017WR020754

Schilling, O.S., D.J. Irvine, H.-J. Hendricks Franssen, and P. Brunner. 2017b. Estimating the spatial extent of unsaturated zones in heterogeneous river-aquifer systems. *Water Resources Research* 53: 10583–10602. https://doi.org/10.1002/2017WR020409

Schomburg, A., O.S. Schilling, C. Guenat, M. Schirmer, R.C. Le Bayon, and P. Brunner. 2018. Topsoil structure stability in a restored floodplain: Impacts of fluctuating water levels, soil parameters and ecosystem engineers. *Science of the Total Environment* 635: 1610–1622. https://doi.org/10.1016/j.scitotenv.2018.05.120

Stefan, J. 1889. Über die Verdampfung und die Auflösung als Vorgänge der Diffusion. *Sitzungsberichte der kaiserlichen Akademie der Wissenschaften Wien. Mathematisch-naturwissenschaftlichen Classe, Abteilung IIa* 98: 1418–1442.

Tang, Q., W. Kurtz, O.S. Schilling, P. Brunner, H. Vereecken, and H.-J. Hendricks Franssen. 2017. The influence of riverbed heterogeneity patterns on river-aquifer exchange fluxes under different connection regimes. *Journal of Hydrology* 554: 383–396. https://doi.org/10.1016/j.jhydrol.2017.09.031

Tang, Q., O.S. Schilling, W. Kurtz, P. Brunner, H. Vereecken, and H.-J. Hendricks Franssen. 2018. Simulating flood induced riverbed transience using unmanned aerial vehicles, physically-based hydrological modelling and the ensemble Kalman filter. *Water Resources Research.* https://doi.org/10.1029/2018WR023067

Therrien, R., and E. Sudicky. 1996. Three-dimensional analysis of variably-saturated flow and solute transport in discretely-fractured porous media. *Journal of Contaminant Hydrology* 23: 1–44. https://doi.org/10.1016/0169-7722(95)00088-7

Voss, C. I., & Provost, A. (2010). SUTRA: A model for saturated-unsaturated variable density groundwater flow with solute or energy transport. *Version 2.2* . Retrieved from Reston, VA

Wang, G., H. Hongchang, and L. Taibin. 2009. The influence of freeze–thaw cycles of active soil layer on surface runoff in a permafrost watershed. *Journal of Hydrology* 375: 438–449. https://doi.org/10.1016/j.jhydrol.2009.06.046

Waylen, P., and M.-K. Woo. 1982. Prediction of annual floods generated by mixed processes. *Water Resources Research* 18, no. 4: 1283–1286. https://doi.org/10.1029/WR018i004p01283

Woo, M.-K. 2008. *Cold Region Atmospheric and Hydrologic Studies. The Mackenzie GEWEX Experience*. vol. *2*: *Hydrologic Processes*. Berlin Heidelberg: Springer-Verlag.

Woo, M.-K., P. Marsh, and J.W. Pomeroy. 2000. Snow, frozen soils and permafrost hydrology in Canada, 1995–1998. *Hydrological Processes* 14, no. 9: 1591–1611. https://doi.org/10.1029/WR018i004p01283

Zeinivand, H., and F. De Smedt. 2010. Prediction of snowmelt floods with a distributed hydrological model using a physical snow mass and energy balance approach. *Natural Hazards* 54: 451–468. https://doi.org/10.1007/s11069-009-9478-9

Zhang, Z., D.L. Kane, and L.D. Hinzmann. 2000. Development and application of a spatially-distributed arctic hydrological and thermal process model (ARHYTHM). *Hydrological Processes* 14: 1017–1044. https://doi.org/10.1002/(SICI)1099-1085(20000430)14:63.0.CO;2-G

Zhang, Y., S.K. Carey, and W.L. Quinton. 2008. Evaluation of the algorithms and parameterizations for ground thawing and freezing simulation in permafrost regions. *Journal of Geophysical Research* 113, no. D17: 1–17. https://doi.org/10.1029/2007JD009343